Scattering by a small object close to an interface. II. Study of backscattering

K. O. Muinonen

Observatory and Astrophysics Laboratory, University of Helsinki, Tähtitorninmäki, SF-00130 Helsinki, Finland

A. H. Sihvola and I. V. Lindell

Electromagnetics Laboratory, Helsinki University of Technology, Otakaari 5 A, SF-02150 Espoo, Finland

K. A. Lumme

Observatory and Astrophysics Laboratory, University of Helsinki, Tähtitorninmäki, SF-00130 Helsinki, Finland

Scattering by a small object located close to an interface is analyzed according to the exact-image theory formulation. The scatterer is assumed to be small compared with wavelength, permitting the electric-dipole approximation, and to have a scalar polarizability. After the derivation of the dipole moment, investigations concentrate on far-field scattering. Backscattering enhancement and reversal of linear polarization are confirmed through statistical averaging over scatterer height and system orientation.

1. INTRODUCTION

In the preceding paper[1] exact-image theory formulation was established for the problem of a small scattering object close to an interface. The present paper concentrates on the special case of an object with scalar polarizability and is a natural continuation of Ref. 1.

In a recent paper on scattering by two small objects in the electric-dipole approximation,[2] backward enhancement was seen to be accompanied by a reversal of linear polarization. Both phenomena were verified in second-order scattering, but, because of the small scattering cross section, they could not be observed in total angular scattering. The other dipole scatterer is replaced here with a material half-space. This increases the weight of second-order scattering so that the phenomena also show up in total scattering.

The motivation for these backscattering studies comes from two almost universal phenomena observed in scattering of sunlight from atmosphereless solar-system bodies. These bodies, most probably covered with inhomogeneous cosmic dust particles, exhibit opposition brightening, i.e., backscattering enhancement, and a reversal of linear polarization near opposition.

As for the opposition brightening, Seeliger made the first efforts to understand the brightening of the Saturnian system in 1887.[3] Rougier reported a wide collection of observations of the lunar phase curve in 1933.[4] Lyot discovered the reversal of linear polarization for Saturn's rings in 1923 and published the linear polarization of the Moon in 1929.[5] Both phenomena have also been observed for interplanetary dust.

Various attempts to explain the observed phenomena have been made during the past century. Only recently it has been suggested that interference in multiple scattering could be responsible for these phenomena.[2,6,7] The interference mechanism is built into Maxwell's equations for electromagnetism and requires only that the scattering medium be inhomogeneous. Backward enhancement already has been investigated in the field of microwave scattering.[8,9]

In Section 2 the dipole moment of the scatterer is derived from the general solution of Ref. 1. Far-field scattering for an unpolarized incident field is presented in Section 3. Backward enhancement and reversal of polarization are studied in Section 4. Conclusions are summarized in Section 5.

2. DIPOLE MOMENT

In the present scattering geometry the incident and the reflected plane waves $\mathbf{E}^i$ and $\mathbf{E}^r$ propagate in the yz plane of the fixed coordinate system xyz and scatter from an object located at $\mathbf{r} = \mathbf{u}_z h$ (Fig. 1). The lower half-space is assumed to be dielectric and nonpermeable with relative permittivity ϵ and with relative permeability $\mu = 1$. The coordinate system $x'y'z'$ is needed in the study of backscattering. It is connected to the direction of the incident field so that the z' axis points in the direction of the source.

The object is assumed to be small compared with wavelength. In this case the induced electric-dipole moment predominates over other multipole moments and gives an accurate description of the scattering characteristics. The incident and reflected fields at the object are

$$\mathbf{E}^i(\mathbf{u}_z h) = \mathbf{E}_0 \exp(j\beta_i h),$$

$$\mathbf{E}^r(\mathbf{u}_z h) = \mathcal{R}_i(\beta_i) \cdot \mathbf{E}_0 \exp(-j\beta_i h),$$

$$\beta_i = k \cos\theta_i, \qquad k^2 = \omega^2 \mu_0 \epsilon_0, \qquad (1)$$

where θ_i is the angle of incidence. The reflection dyadic $\mathcal{R}_i$ can here be reduced [from Eqs. (5)–(7) of Ref. 1] to
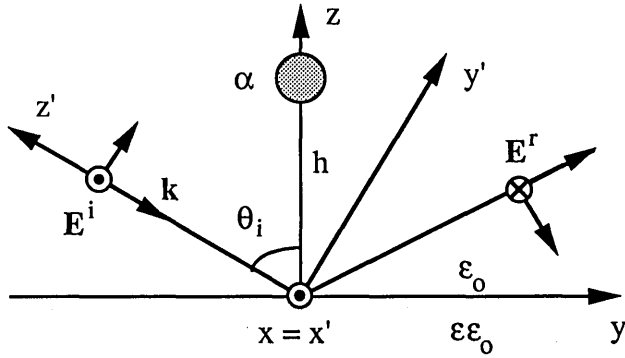
Fig. 1. Scattering geometry. The incident and the reflected fields propagate in the *yz* plane and scatter from a small object. Notice the fixed and incidence-dependent (primed) coordinate systems.

$$\mathcal{R}_i(\beta_i) = \mathbf{u}_x\mathbf{u}_x R^{\mathrm{TE}}(\beta_i) + \mathbf{u}_y\mathbf{u}_y R^{\mathrm{TM}}(\beta_i) - \mathbf{u}_z\mathbf{u}_z R^{\mathrm{TM}}(\beta_i), \quad (2)$$

with Fresnel coefficients

$$R^{\mathrm{TE}}(\beta_i) = \frac{\beta_i - \beta_1}{\beta_i + \beta_1},$$

$$R^{\mathrm{TM}}(\beta_i) = -\frac{\epsilon\beta_i - \beta_1}{\epsilon\beta_1 + \beta_1}, \quad \beta_1 = k\left(\epsilon - 1 + \frac{\beta_i^2}{k^2}\right)^{1/2}. \quad (3)$$

For a sphere of radius *a* and scalar polarizability α, the dyadic polarizability

$$\alpha = \alpha\mathcal{J} = 4\pi\epsilon_0\frac{\epsilon_s - 1}{\epsilon_s + 2}a^3\mathcal{J}, \quad (4)$$

where ϵ_s is the relative permittivity and $\mathcal{J}$ is the unit dyadic.[10] Note that the vacuum permittivity ϵ_0 is included in the polarizability α.

In Eq. (30) of Ref. 1 the electric-dipole moment was seen to be related to the incident and the reflected fields by

$$\mathbf{p} = [\mathcal{J} - \omega^2\mu_0\alpha \cdot \mathcal{H}(\mathbf{u}_z 2h) \cdot \mathcal{C}]^{-1} \cdot \alpha \cdot [\mathbf{E}^i(\mathbf{u}_z h) + \mathbf{E}^r(\mathbf{u}_z h)], \quad (5)$$

where the mirror dyadic $\mathcal{C}$ is

$$\mathcal{C} = \mathcal{J}_t - \mathbf{u}_z\mathbf{u}_z,$$

$$\mathcal{J}_t = \mathbf{u}_x\mathbf{u}_x + \mathbf{u}_y\mathbf{u}_y. \quad (6)$$

Accordingly, $\mathcal{J}_t$ is the transverse unit dyadic. The Green's dyadic $\mathcal{H}$ accounts for the influence of the interface,

$$\mathcal{H}(\mathbf{u}_z 2h) = \mathcal{J}_t K_t(2h) + \mathbf{u}_z\mathbf{u}_z K_z(2h), \quad (7)$$

and its complex-valued components K_t and K_z depend on the permittivity of the lower half-space and are presented in detail in Eq. (34) of Ref. 1. They are oscillating functions of *kh* that asymptotically approach zero with increasing *kh*.

After inserting Eqs. (4), (6), and (7) into Eq. (5) and inverting the diagonal dyadic, we obtain

$$\mathbf{p} = \mathcal{Q}(\mathbf{u}_z 2h) \cdot [\mathbf{E}^i(\mathbf{u}_z h) + \mathbf{E}^r(\mathbf{u}_z h)], \quad (8)$$

where the $\mathcal{Q}$ dyadic is

$$\mathcal{Q}(\mathbf{u}_z 2h) = \mathcal{J}_t Q_t(2h) + \mathbf{u}_z\mathbf{u}_z Q_z(2h),$$

$$Q_t(2h) = \frac{\alpha}{1 - \omega^2\mu_0\alpha K_t(2h)},$$

$$Q_z(2h) = \frac{\alpha}{1 + \omega^2\mu_0\alpha K_z(2h)}. \quad (9)$$

The $\mathcal{Q}$ dyadic is termed the effective dyadic polarizability since it replaces the polarizability dyadic α. It accounts for the interface through the Green's dyadic components K_t and K_z. The solution for the dipole moment resembles the one obtained for two isolated dipole scatterers.[2]

It is straightforward to spell out the relation between the amplitude of the incident plane wave $\mathbf{E}_0$ and the induced dipole moment $\mathbf{p}$. Inserting Eq. (1) into Eq. (8), we readily obtain

$$\mathbf{p} = [\exp(j\beta_i h)\mathcal{Q} + \exp(-j\beta_i h)\mathcal{Q} \cdot \mathcal{R}_i] \cdot \mathbf{E}_0. \quad (10)$$

The interaction between the scattering object and the lower half-space has been collected into the dyadic in front of the incident amplitude. The order of scattering is defined according to the powers of the polarizability and Fresnel coefficients. Thereby, the dyadic $\mathcal{Q}$ includes terms starting from the first order, whereas the dyadic $\mathcal{Q} \cdot \mathcal{R}_i$ is already of the second order.

3. SCATTERED FAR FIELD

The scattered field consists of the fields from the object and the image. The far field of the object can be obtained from the current density $\mathbf{J}$ with the help of the free-space Green's dyadic $\mathcal{G}$,[11]

$$\mathbf{E}_1{}^s(\mathbf{r}) = -j\omega\mu_0\int_V dV''\mathcal{G}(\mathbf{r} - \mathbf{r}'') \cdot \mathbf{J}(\mathbf{r}'')$$

$$= -j\omega\mu_0\int_V dV''\mathcal{G}(\mathbf{r} - \mathbf{r}'') \cdot j\omega p\delta(\mathbf{r}'' - \mathbf{u}_z h)$$

$$\rightarrow \omega^2\mu_0 G(\mathbf{r})\exp(j\beta_s h)\mathcal{J}_s \cdot \mathbf{p}, \quad kr \gg 1, \quad (11)$$

where the Green's functions are explicitly

$$\mathcal{G}(\mathbf{r}) = \left(\mathcal{J} + \frac{1}{k^2}\nabla\nabla\right) \cdot G(\mathbf{r}),$$

$$G(\mathbf{r}) = \frac{\exp[-jkD(\mathbf{r})]}{4\pi D(\mathbf{r})}, \quad D(\mathbf{r}) = (\mathbf{r} \cdot \mathbf{r})^{1/2}. \quad (12)$$

Using the spherical coordinates ϑ, φ of the *xyz* coordinate system, we see that

$$\mathcal{J}_s = \mathbf{u}_\vartheta\mathbf{u}_\vartheta + \mathbf{u}_\varphi\mathbf{u}_\varphi,$$

$$\beta_s = k\cos\vartheta. \quad (13)$$

Thus $\mathcal{J}_s$ is the unit dyadic transverse to the scattering direction.

The scattered far field of the image can be obtained from the mirror current density $\mathbf{J}_c$ with the help of the Green's dyadic $\mathcal{H}$ as in Eq. (27) of Ref. 1:

$$\mathbf{E}_2{}^s(\mathbf{r}) = -j\omega\mu_0\int_V dV''\mathcal{H}(\mathbf{r} - \mathbf{r}'') \cdot \mathbf{J}_c(\mathbf{r}'')$$

$$= -j\omega\mu_0\int_V dV''\mathcal{H}(\mathbf{r} - \mathbf{r}'') \cdot \mathcal{C} \cdot j\omega p\delta(\mathbf{r}'' + \mathbf{u}_z h)$$

$$\rightarrow \omega^2\mu_0 G(\mathbf{r})\exp(-j\beta_s h)\mathcal{R}_s(\beta_s) \cdot \mathbf{p}, \quad kr \gg 1, \quad (14)$$

where the reflection dyadic $\mathcal{R}_s$ is

$$\mathcal{R}_s(\beta_s) = [\mathbf{u}_\vartheta \mathbf{u}_\vartheta R^{\mathrm{TM}}(\beta_s) + \mathbf{u}_\varphi \mathbf{u}_\varphi R^{\mathrm{TE}}(\beta_s)] \cdot \mathcal{C}. \quad (15)$$

The far fields in Eqs. (11) and (14) resemble each other to a great extent. In the far field of the image, the unit dyadic has been replaced with a reflection dyadic, and the phase factor is the complex conjugate of the one in Eq. (11).

The total scattered far field is the sum of the fields from the scatterer and the image,

$$\mathbf{E}^s(\mathbf{r}) = \mathbf{E}_1^s(\mathbf{r}) + \mathbf{E}_2^s(\mathbf{r})$$

$$= \omega^2 \mu_0 G(\mathbf{r})[\exp(j\beta_s h)\mathcal{I}_s + \exp(-j\beta_s h)\mathcal{R}_s(\beta_s)] \cdot \mathbf{p}$$

$$\equiv \omega^2 \mu_0 G(\mathbf{r})\mathbf{A}, \quad (16)$$

including the definition for the scattering amplitude **A**. Showing the dyadic operations explicitly, we find, with the help of Eqs. (10) and (16), that

$$\mathbf{A} = \{\exp[j(\beta_i + \beta_s)h]\mathcal{I}_s \cdot \mathcal{Q} + \exp[-j(\beta_i - \beta_s)h]\mathcal{I}_s \cdot \mathcal{Q} \cdot \mathcal{R}_i$$

$$+ \exp[j(\beta_i - \beta_s)h]\mathcal{R}_s \cdot \mathcal{Q} + \exp[-j(\beta_i + \beta_s)h]\mathcal{R}_s \cdot \mathcal{Q} \cdot \mathcal{R}_i\} \cdot \mathbf{E}_0. \quad (17)$$

Using Eqs. (3) and (15), we see that the scattering amplitude vanishes for $\beta_s = 0$, i.e., in the xy plane.

After calculating the scattering amplitude for incident polarizations perpendicular (TE) and parallel (TM) to the yz plane of incidence, we obtain the scattering function S for unpolarized incident field:

$$S(\vartheta, \varphi) = \frac{1}{2} \frac{|\mathbf{A}^{\mathrm{TE}}|^2 + |\mathbf{A}^{\mathrm{TM}}|^2}{|\mathbf{E}_0|^2}. \quad (18)$$

In Figs. 2–4 the total and second-order scattering functions are shown for normalized scatterer heights $kh = \pi/2, \pi, 2\pi$ and for the incidence angle $\theta_i = 45°$. The present second-order function includes contributions from the second and third terms in Eq. (17). Figure 2 indicates an interesting
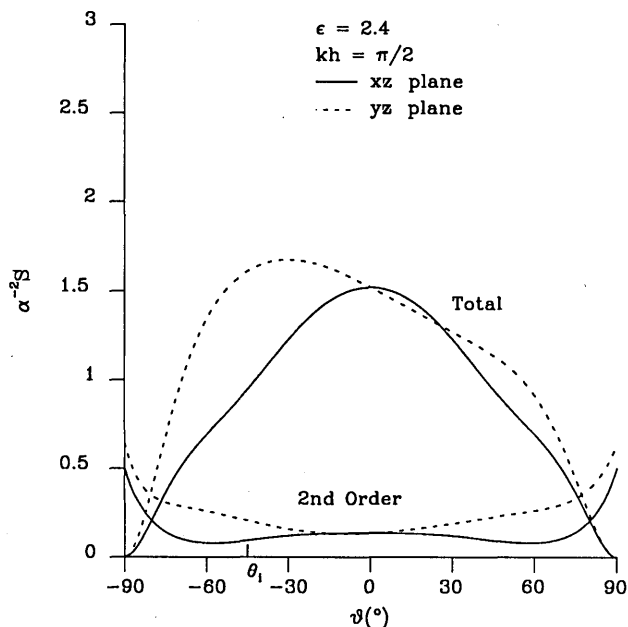

Fig. 2. Total and second-order scattering by a spherical object at $kh = \pi/2$ according to Eq. (18) for an unpolarized incident field with incidence angle $\theta_i = 45°$. See text for scattering into grazing angles.
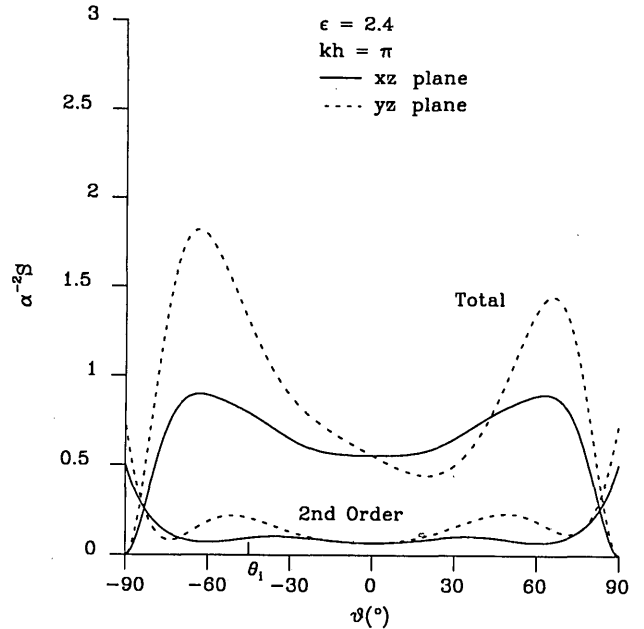

Fig. 3. Same as Fig. 2 for $kh = \pi$. Note the asymmetry of total scattering in the yz plane of incidence.
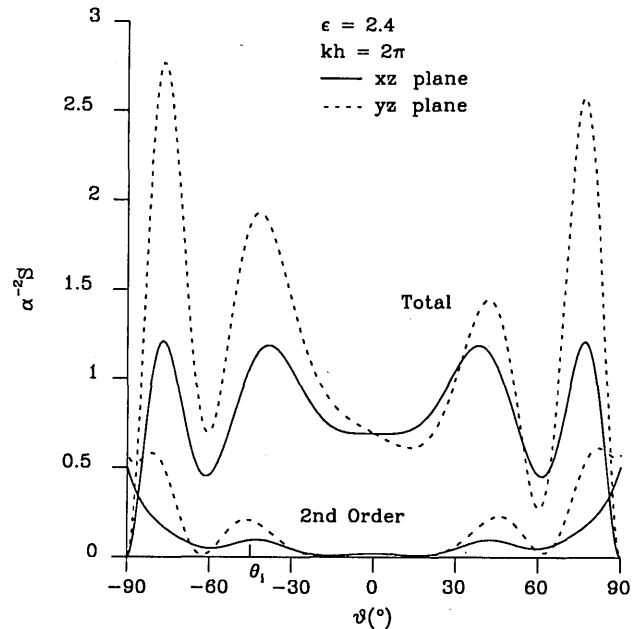

Fig. 4. Same as Fig. 2 for $kh = 2\pi$. Notice the formation of backward enhancement in second-order scattering.

artifact: near a 90° scattering angle, the second-order intensity exceeds the total one. Thus great care must be taken when separating different orders of scattering without regard to phase, i.e., in a geometrical optics sense. Note the gradual increase of backscattering for the second order, shown in Figs. 3 and 4.

4. BACKWARD ENHANCEMENT AND POLARIZATION REVERSAL

In order to reach an understanding of the backscattering phenomena observed for inhomogeneous particulate media,

we introduce statistical averaging over surface slopes and over the height of the scattering object. The probability density for height is assumed to be a gamma distribution with integer γ (Ref. 12):

$$p_h(h)dh = \frac{1}{(\gamma - 1)!}\left(\frac{\gamma}{h_0}\right)^\gamma h^{\gamma-1} \exp\left(-\frac{\gamma h}{h_0}\right)dh, \qquad (19)$$

where h_0 is the mean height. For this distribution, the standard deviation of height is $h_0/\sqrt{\gamma}$ and decreases with increasing γ. The gamma distribution is an appropriate choice since it decreases the effect of long-range interactions, which tend to be shadowed in a real dust layer. Orientation averaging is then carried out by making use of the isotropic Gaussian probability density for slope ($t = \tan\theta_i$; e.g., see Ref. 9):

$$p_t(t)dtd\phi_i = \frac{1}{2\pi\rho^2}\exp\left(-\frac{t^2}{2\rho^2}\right)tdtd\phi_i$$

$$= \frac{1}{2\pi\rho^2}\exp\left(-\frac{\tan^2\theta_i}{2\rho^2}\right)\frac{\sin\theta_i}{\cos^3\theta_i}d\theta_i d\phi_i, \qquad (20)$$

where ρ is the standard deviation of slope. Thereby, only normal incidence to a rough surface is considered. The gamma and Gaussian distributions have been selected because of their simplicity. The emphasis here is not on detailed but rather on broad-minded modeling of natural circumstances.

Let us define the amplitude components:

$$A_\theta \equiv \Theta_1 \exp[j(\beta_i + \beta_s)h] + \Theta_2 \exp[-j(\beta_i - \beta_s)h]$$

$$+ \Theta_3 \exp[j(\beta_i - \beta_s)h] + \Theta_4 \exp[-j(\beta_i + \beta_s)h],$$

$$A_\phi \equiv \Phi_1 \exp[j(\beta_i + \beta_s)h] + \Phi_2 \exp[-j(\beta_i - \beta_s)h]$$

$$+ \Phi_3 \exp[j(\beta_i - \beta_s)h] + \Phi_4 \exp[-j(\beta_i + \beta_s)h], \qquad (21)$$

where θ and ϕ are spherical coordinates in the $x'y'z'$ system (Fig. 1). This definition permits the investigation on the influence of different phase factors. The coefficient functions can be obtained from Eq. (17) through corresponding scalar product operations, for example,

$$\Theta_1 = \mathbf{u}_\theta \cdot \mathcal{Q} \cdot \mathbf{E}_0,$$

$$\Theta_2 = \mathbf{u}_\theta \cdot \mathcal{Q} \cdot \mathcal{R}_i \cdot \mathbf{E}_0,$$

$$\Theta_3 = \mathbf{u}_\theta \cdot \mathcal{R}_s \cdot \mathcal{Q} \cdot \mathbf{E}_0,$$

$$\Theta_4 = \mathbf{u}_\theta \cdot \mathcal{R}_s \cdot \mathcal{Q} \cdot \mathcal{R}_i \cdot \mathbf{E}_0. \qquad (22)$$

The evaluation of these functions requires knowledge of the coordinate transformations

$$\sin\vartheta \cos\varphi = \sin\theta \cos\phi,$$

$$\sin\vartheta \sin\varphi = \sin\theta \sin\phi \cos\theta_i - \cos\theta \sin\theta_i,$$

$$\cos\vartheta = \sin\theta \sin\phi \sin\theta_i + \cos\theta \cos\theta_i \qquad (23)$$

between the xyz and $x'y'z'$ coordinate systems. Note that the $x'y'z'$ system has been defined in such a way that the transformations in Eqs. (23) are independent of ϕ_i. This is justified by the fact that, for normal incidence, averaging over the incidence angle ϕ_i can be replaced by averaging over the scattering angle ϕ.

The averaged scattering function and degree of linear polarization for an unpolarized incident field are defined as

$$S(\theta) = \frac{1}{2|\mathbf{E}_0|^2}\langle |A_\theta^{TE}|^2 + |A_\theta^{TM}|^2 + |A_\phi^{TE}|^2 + |A_\phi^{TM}|^2\rangle,$$

$$P(\theta) = -\frac{\langle |A_\theta^{TE}|^2 + |A_\theta^{TM}|^2 - |A_\phi^{TE}|^2 - |A_\phi^{TM}|^2\rangle}{\langle |A_\theta^{TE}|^2 + |A_\theta^{TM}|^2 + |A_\phi^{TE}|^2 + |A_\phi^{TM}|^2\rangle}, \qquad (24)$$

where, for example,

$$\langle |A_\theta^{TE}|^2\rangle = \int_0^\infty dh p_h(h) \int_0^\infty dt \int_0^{2\pi} d\phi_i p_t(t, \phi_i)|A_\theta^{TE}|^2. \qquad (25)$$
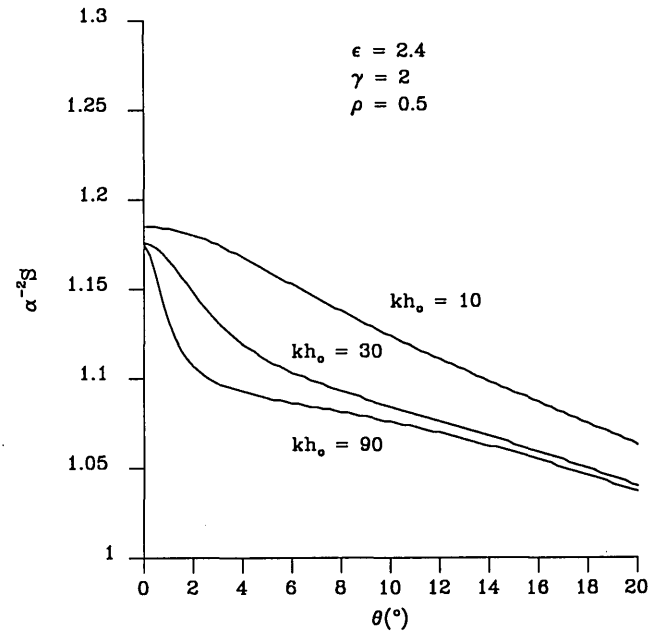

Fig. 5. Slight backward enhancement in averaged total scattering. The enhancement is due mainly to second-order scattering.
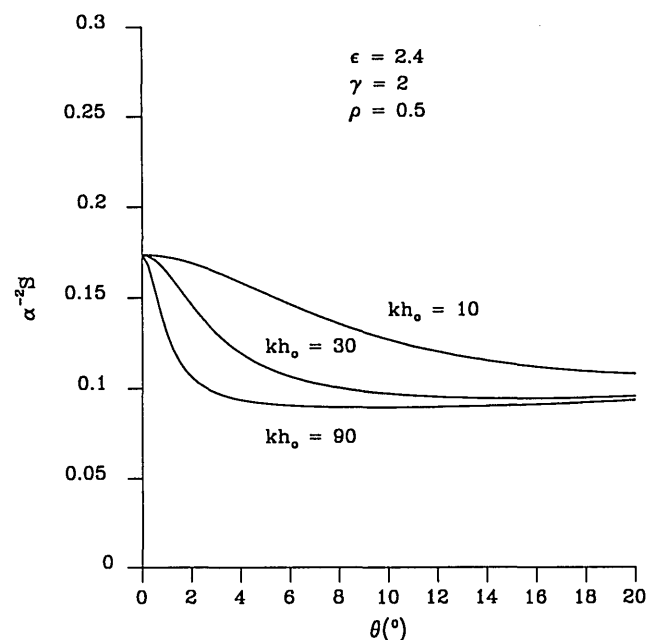

Fig. 6. Backward enhancement in averaged second-order scattering. Note the sharpening of the peak with increasing mean height.
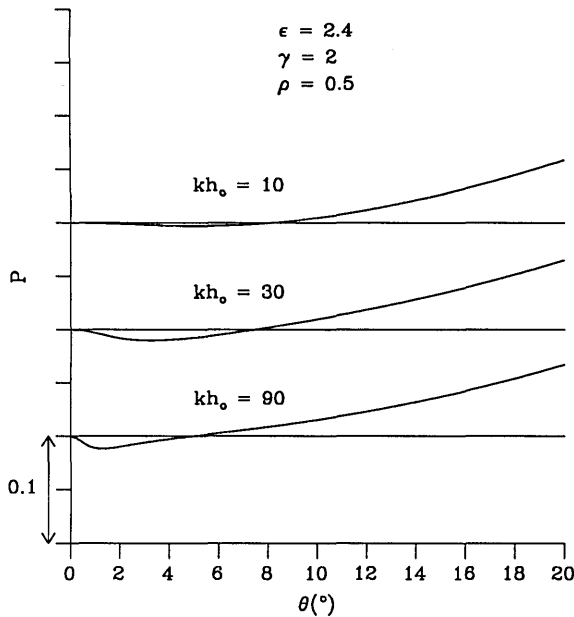
Fig. 7. Reversal of linear polarization in averaged total scattering. The horizontal lines indicate zero-polarization levels.
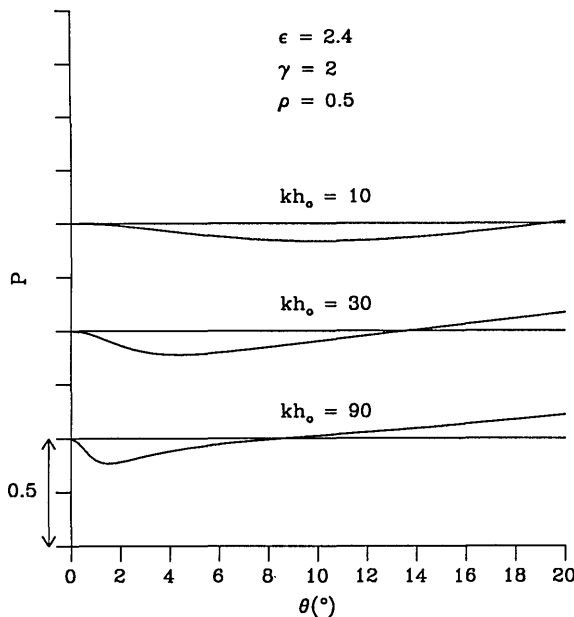

Fig. 8. Reversal of linear polarization in averaged second-order scattering. Note the widening of the negative branch with decreasing mean height.

As mentioned above, the integration over ϕ_i can be replaced by an integration over ϕ. It is obvious that shadowing plays a major role in the case of high standard deviation ρ. In order to avoid that difficulty, we use rather small standard deviations $\rho \le 0.5$ in the following orientation averaging.

As for height averaging, using the Green's function derived in Ref. 1 (see Figs. 2–5) and the definition for scalar polarizability in Eq. (4), we have

$$\omega^2 \mu_0 \alpha K_t = 4\pi k^3 a^3 \frac{\epsilon_s - 1}{\epsilon_s + 2} \frac{K_t}{k} < 10^{-4} \ll 1, \qquad (26)$$

when $ka < 0.1$, $\epsilon_s < 2.4$, and $kh > 1$. If these conditions are satisfied, the interaction dyadic is practically the same as the dyadic polarizability $Q \approx \alpha$. The only height dependence is now in the exponential phase factors, and averaging over height can be carried out analytically:

$$\langle |A_\theta|^2 \rangle_h = |\Theta_1|^2 + |\Theta_2|^2 + |\Theta_3|^2 + |\Theta_4|^2 + 2\mathrm{Re}\{(\Theta_1{}^*\Theta_2 + \Theta_3{}^*\Theta_4)$$
$$\times \langle \exp(-j2\beta_i h) \rangle_h + (\Theta_1{}^*\Theta_3 + \Theta_2{}^*\Theta_4)\langle \exp(-j2\beta_s h) \rangle_h$$
$$+ \Theta_1{}^*\Theta_4 \langle \exp[-j2(\beta_i + \beta_s)h] \rangle_h + \Theta_2{}^*\Theta_3 \langle \exp[j2(\beta_i - \beta_s)h] \rangle_h \}$$
$$(27)$$

and similarly for $\langle |A_\phi|^2 \rangle_h$. The averaged phase factors can be evaluated from

$$\langle \exp(j2\beta h) \rangle_h = \int_0^\infty \mathrm{d}h p_h(h) \exp(j2\beta h)$$

$$= \frac{1}{\left(1 - j\dfrac{2\beta h_0}{\gamma}\right)^\gamma}, \qquad (28)$$

which is the characteristic function of the gamma distribution. As seen from Eq. (28), statistical averaging cancels the incoherent intensity components. The last term in Eq. (27) and the corresponding term in $\langle |A_\phi|^2 \rangle_h$ cause the backward enhancement and the polarization reversal. The factor $\beta = \beta_i - \beta_s$ vanishes at the exact backward direction, causing coherent backscatter. However, it differs from zero for $\theta_i \ne \vartheta$, so that the weight of the corresponding terms rapidly decreases. The reversal of linear polarization arises from the different peak widths in the azimuthal and polar directions.

Figures 5–8 show the effects of backscattering enhancement and reversal of linear polarization in total and second-order scattering. The second order consists of terms including only Θ_2, Θ_3, Φ_2, or Φ_3. Like two dipole scatterers,[2] first-order scattering decreases the magnitude of negative polarization. However, in the present case, negative polarization and backward enhancement show up also in total scattering, which did not happen for two discrete dipole scatterers. Still, it is worth emphasizing that the specular reflection component has been excluded. Negative polarization branch grows wider with increasing standard deviation of slope. For $\rho = 0.5$, shadowing and boundary phenomena (see Figs. 2–4) play a negligible role.

5. CONCLUSIONS

An analytical solution has been presented for electromagnetic scattering by a small scatterer with scalar polarizability located close to an interface. The exact-image theory formulation of the problem has proved to be an efficient and practical way of treating scatterers in the neighborhood of a dielectric half-space.

Backscattering enhancement and reversal of linear polarization have been quantitatively verified in averaged total scattering. The widths of the calculated branches of negative polarization are smaller than the ones observed for solar-system objects. Qualitatively, this suggests that the predominating contribution to opposition phenomena comes from interactions between small-scale inhomogeneities

rather than interactions between small-scale inhomogeneities and smooth-surface elements.

The present results offer a valid basis for the modeling of light scattering from atmosphereless solar-system bodies, planetary rings, and interplanetary and cometary dust.

REFERENCES

1. I. V. Lindell, A. H. Sihvola, K. O. Muinonen, and P. W. Barber, "Scattering by a small object close to an interface. I. Exact-image theory formulation," J. Opt. Soc. Am. A **8**, 472–476 (1991).
2. K. O. Muinonen, "Electromagnetic scattering by two interacting dipoles," in *Proceedings of the 1989 URSI EM Theory Symposium* (International Union of Radio Science, Brussels, 1989), pp. 428–430.
3. H. von Seeliger, "Zur Theorie der Beleuchtung der grossen Planeten, Insbesondere des Saturn," Abh. Bayer. Akad. Wissen. Math. Naturwiss. Kl. **16**, 405–516 (1887).
4. A. Rougier, "Photométrie photoélectrique globale de la Lune," Ann. Obs. Strasbourg **2**, 205–339 (1933).
5. B. Lyot, "Recherches sur la polarisation de la lumière des planètes et de quelques substances terrestres," Ann. Obs. Paris **8**, 1–161 (1929).
6. Y. G. Shkuratov, "Diffractional model of the brightness surge of complex structure surfaces," Kinemat. Fis. Nebesnyh Tel **4**, 33–39 (1988).
7. Y. G. Shkuratov, N. V. Opanasenko, and L. Y. Melkumova, "Interference surge of backscattering and negative polarization of light reflected by complex structure," Preprint 361 (Institute of Radiophysics and Electronics, Academy of Sciences, Kharkov, USSR, 1989), pp. 1–26.
8. S. M. Rytov, Y. A. Kravtsov, and V. I. Tatarskii, *Principles of Statistical Radiophysics 1-4* (Springer-Verlag, Berlin, 1989).
9. L. Tsang, J. A. Kong, and R. T. Shin, *Theory of Microwave Remote Sensing* (Wiley, New York, 1985).
10. C. F. Bohren and D. R. Huffman, *Absorption and Scattering of Light by Small Particles* (Wiley, New York, 1983).
11. I. V. Lindell and E. Alanen, "Exact image theory for the Sommerfeld half-space problem, part III: general formulation," IEEE Trans. Antennas Propag. **32**, 1027–1032 (1989).
12. M. Abramowitz and I. A. Stegun, eds., *Handbook of Mathematical Functions* (Dover, New York, 1965).